RESEARCH ARTICLE



WILEY

Field-based robotic leaf angle detection and characterization of maize plants using stereo vision and deep convolutional neural networks

Lirong Xiang^{1,2} | Jingyao Gai¹ | Yin Bao¹ | Jianming Yu³ | Patrick S. Schnable³ Lie Tang¹ (5)

Correspondence

Lie Tang, Department of Agricultural and Biosystems Engineering, Iowa State University, Ames, IA 50011, USA. Email: lietang@iastate.edu

Present addresses

Jingyao Gai, College of Mechatronic Engineering, Guanxi University, Nanning, 530007, China.

Yin Bao, Department of Biosystems Engineering, Auburn University, Auburn, AL 36849, USA.

Funding information

Plant Sciences Institute at Iowa State University; National Science Foundation Major Research Instrumentation Program; Iowa Agriculture Experiment Station

Abstract

Maize (Zea mays L.) is one of the three major cereal crops in the world. Leaf angle is an important architectural trait of crops due to its substantial role in light interception by the canopy and hence photosynthetic efficiency. Traditionally, leaf angle has been measured using a protractor, a process that is both slow and laborious. Efficiently measuring leaf angle under field conditions via imaging is challenging due to leaf density in the canopy and the resulting occlusions. However, advances in imaging technologies and machine learning have provided new tools for image acquisition and analysis that could be used to characterize leaf angle using three-dimensional (3D) models of field-grown plants. In this study, PhenoBot 3.0, a robotic vehicle designed to traverse between pairs of agronomically spaced rows of crops, was equipped with multiple tiers of PhenoStereo cameras to capture sideview images of maize plants in the field. PhenoStereo is a customized stereo camera module with integrated strobe lighting for high-speed stereoscopic image acquisition under variable outdoor lighting conditions. An automated image processing pipeline (AngleNet) was developed to measure leaf angles of nonoccluded leaves. In this pipeline, a novel representation form of leaf angle as a triplet of keypoints was proposed. The pipeline employs convolutional neural networks to detect each leaf angle in two-dimensional images and 3D modeling approaches to extract quantitative data from reconstructed models. Satisfactory accuracies in terms of correlation coefficient (r) and mean absolute error (MAE) were achieved for leaf angle (r > 0.87, MAE < 5°) and internode heights (r > 0.99, MAE < $3.5 \, \mathrm{cm}$). Our study demonstrates the feasibility of using stereo vision to investigate the distribution of leaf angles in maize under field conditions. The proposed system is an efficient alternative to traditional leaf angle phenotyping and thus could accelerate breeding for improved plant architecture.

KEYWORDS

convolutional neural network, field-based plant phenotyping, keypoint detection, leaf angle, stereo vision

This is an open access article under the terms of the Creative Commons Attribution-NonCommercial-NoDerivs License, which permits use and distribution in any medium, provided the original work is properly cited, the use is non-commercial and no modifications or adaptations are made.

© 2023 The Authors. *Journal of Field Robotics* published by Wiley Periodicals LLC.

J Field Robotics. 2023;1–20. wileyonlinelibrary.com/journal/rob

¹Department of Agricultural and Biosystems Engineering, Iowa State University, Ames, Iowa, USA

²Department of Biological and Agricultural Engineering, North Carolina State University, Raleigh, North Carolina, USA

³Department of Agronomy, Iowa State University, Ames, Iowa, USA



1 | INTRODUCTION

Improving plant productivity and efficiency has become an important mission of plant breeding with the ever-increasing world population and climate change (Furbank & Tester, 2011). Understanding the adaptation of plants to various environments relies on dissecting the relationship between plant genotype (underlying genetic codes) and phenotype (e.g., plant architecture). Such knowledge can potentially aid in developing productive crop varieties and accelerate the plant breeding progress (Gibbs et al., 2018). Given the importance of maize as a cereal crop, plant breeders strive to generate high-yielding, stress-tolerant maize varieties (Che et al., 2020; N. Wang et al., 2015). Plant architecture plays an essential role in the interception of solar radiation (Duan et al., 2016; Truong et al., 2015). However, maize leaves are curved and this complicates how leaf curvature can be described by a single system of equations (Ford et al., 2008). Leaf curvature is influenced by not only ligule formation and growth, but also other factors including stiffness of the leaf material, midrib structure, vein density, leaf width, and length (Ford et al., 2008). As major part of leaf curvature, leaf angle, has attracted attention over decades for increasing crop yields (Lewis et al., 2014; Pendleton et al., 1968). Leaf angle is defined as the angle between the plant stem and leaf adaxial side of the blade (D. Tang et al., 2018). An optimal arrangement of leaves from the top to the bottom of the canopy can increase photosynthetic efficiency, thereby potentially increasing grain yield per unit area (Dzievit et al., 2019; Mantilla-Perez et al., 2020; Ort et al., 2015). Leaf angle is associated with increased productivity in maize (Hammer et al., 2009; Lewis et al., 2014; Mansfield & Mumm, 2014; X.-G. Zhu et al., 2010). A canopy configuration with leaves at a more horizontal angle in the lower canopy and a more upright angle in the upper canopy is most desirable (Dzievit et al., 2019; X. Zhang et al., 2017).

Breeding for leaf angle requires measuring the leaf angles of large numbers of field-grown plants. The most common method is to select representative plants and manually measure the angles of typical leaves (Dzievit et al., 2019; Zhao et al., 2018). This slow process often fails to capture variation among leaf angles from the upper to lower portions of the crop canopy. Therefore, there is an urgent need to develop automated, high-throughput phenotyping methods for leaf angle (Mantilla-Perez et al., 2020; X. Zhang et al., 2017).

Advances in high-throughput plant phenotyping platforms and sensing technologies provide an opportunity to improve the efficiency of leaf angle measurement (Chen et al., 2021; Duan et al., 2016; Mccormick et al., 2016; Y. Tang et al., 2020). Several studies on methods for automated leaf angle measurements in maize plants using two-dimensional (2D) and three-dimensional (3D) images under controlled environments have recently been reported. For 2D imaging, RGB cameras are extensively used in indoor phenotyping systems to capture side-view images of maize plants (Cabrera-Bosquet et al., 2016; Kenchanmane Raju et al., 2020; X. Zhang et al., 2017). Most of the previous studies used binarization-skeletonization method for leaf segmentation and requires controlled

light conditions and viewing angles for image acquisition (Das Choudhury et al., 2018; Kenchanmane Raju et al., 2020; Souza et al., 2021). For example, Cabrera-Bosquet et al. (2016) used the PHENOARCH platform equipped with RGB cameras to capture 12 side-view images of a single maize plant; the image with the most information was selected for leaf angle measurement. These 2D imaging-based methods have a high throughput, but they require a camera pose where the leaf-stem plane is parallel to the image plane to get accurate leaf angle measurement and are therefore not suitable for in-field leaf angle measurements. In contrast, 3D imaging that includes depth information provides the opportunity to overcome the limitations of 2D approaches (Apelt et al., 2015; Sun et al., 2020). Several technologies have been developed to reconstruct maize canopies and measure leaf angle in 3D space, such as 3D laser scanning (Y. Wang et al., 2019), light detection and ranging (LiDAR) (Thapa et al., 2018), structure from motion (Zermas et al., 2020), and time-of-flight (ToF) imaging (Chaivivatrakul et al., 2014). Y. Wang et al. (2019) compared the representative 3D data acquisition approaches for maize phenotyping and obtained reliable measurements of leaf angle. The skeletonization approach has also been successfully used for interpreting the structure of 3D canopies, where a 3D skeleton was created by point cloud slicing along the growth direction (Bao, Tang, Breitzman, et al., 2019; Xiang et al., 2019; Zermas et al., 2020), or voxel thinning (Gaillard et al., 2020), or Laplacian contraction (Wu et al., 2019; C. Zhu et al., 2020). However, the existing methods for detecting and measuring leaf angle are more effective for maize plants with fully expanded and sparsely distributed leaves, and have limited ability to address the challenges in segmenting severely overlapped leaves in the field.

Developing field-based high-throughput phenotyping systems for agronomically grown maize plants remains difficult because of the field and crop conditions including: (1) Narrow row spacing: agronomically spaced maize crop rows are typically 0.76 m apart in the United States, and therefore, the robotic vehicle must have a narrow-body to traverse between crop rows and the imaging sensor must have a short working distance to acquire side-view images of maize plants; (2) Extreme plant height: Some maize plants can grow 3-m tall and more, requiring multiple tiers of imaging sensors to cover the whole plant within the narrow agronomic row spacing; (3) Uneven ground surface: Running a narrow vehicle to image tall maize plants in a close vicinity on uneven field surfaces demands real-time balancing of the sensor mast; (4) Occlusion of plant canopies: There are serious occlusions of the plant organs (e.g., leaves, stalks) toward the imaging sensors due to either plant orientation or interferences from the neighboring plants, making 3D image analysis a necessity; (5) Environmental variations: variable lighting and wind conditions in the field can complicate the acquisition of high-quality images. Hence, the image sensor should have a high shutter speed and consistent lighting to overcome motion blur and variable lighting. Stereo vision with an active strobe lighting system provides a practical way for such purpose.

15564967, 0, Downloaded from https://onlinelibrary.wiley.com/doi/10.1002/rob.22166, Wiley Online Library on [01/07/2023]. See the Terms and Conditions (https://onlinelibrary.wiley.com/terms-and-conditions) on Wiley Online Library for rules of use; OA articles are governed by the applicable Creative Commons

The leaf angle characterization of field-grown maize plants is regarded as one of the most challenging phenotyping tasks because of the substantial overlap and occlusion in maize plant canopies; and moreover, variable stem and leaf orientations relative to the camera can affect their visibility near a leaf collar (Bao, Tang, Srinivasan, et al., 2019). To address these challenges, Wu et al. (2019) transported maize plants from the field to the greenhouse for 3D scanning, the resultant point cloud was first preprocessed manually and then skeletonized for leaf segmentation. As noted in the study, the 3D scanner is sensitive to wind, and even light wind caused by human moving would lead to overlaps and offsets in the point cloud. Additionally, the image acquisition process is a fairly low-throughput and therefore not feasible for in-field applications. To measure maize plants in the field, Bao, Tang, Srinivasan, et al. (2019) developed an automated system to characterize plant architectural traits based on ToF 3D imaging. Plants were detected as 3D Hough lines and a skeletonization algorithm was developed to separate stems and leaves. However, the estimation of leaf angle suffered from occlusion and overlapped canopies especially for the plants at late growth stages. Additionally, this method requires increased interrow and intra-row spacing to reduce occlusions and to achieve a sufficient field of view for the depth camera, and the images must be acquired near or after sunset due to the ToF camera's susceptibility to sunlight. Due to the dense canopy and severe occlusion, especially during later periods of plant growth, the segmentation of individual plants and leaves can be difficult when plants are grown at agronomic field densities. Therefore, several plot-level architectural traits such as plot-based plant width (PPW) (Mantilla-Perez et al., 2020) have been developed to estimate leaf angle indirectly. However, such plot-level descriptors can be influenced by other architectural traits: for example, longer leaves with the same leaf angles may result in a larger PPW value. This method of leaf angle measurement was seriously compromised because the severe occlusions generated by the dense plant population and dense canopy of sorghum plants have made automated leaf angle detection largely impossible. To the best of our knowledge, no previous studies have been reported on automatically measuring leaf angle of maize plants in the field with 30-inch row spacing.

Following recent breakthroughs, deep convolutional neural networks (CNNs) have strong performance on image processing tasks in field-based plant phenotyping studies (Pérez-Borrero et al., 2020; Santos et al., 2020; Zou et al., 2020). Compared with traditional computer vision methods, CNN-based approaches can better cope with the image-by-image variations caused by the differences in occlusion, illumination, and viewpoints, hence providing new opportunities for automation (Koirala et al., 2019; Vit et al., 2020). The morphological trait characterization step in plant phenotyping can be treated as an object detection problem, in which CNN models can be trained to find the regions or points of interest (Jiang & Li, 2020). For example, in a study measuring stem diameter in sorghum plants in the field, a region-based CNN model was used to detect sorghum stems in a given image (Xiang et al., 2020). In another study, this model was used to identify points for length phenotyping (Vit et al., 2020).

We focused on the problems associated with detecting and measuring leaf angles along the entire height of maize plants based on 3D models reconstructed from stereoscopic images. Motivated by keypoint-based human-pose estimation, the topology of a leaf angle was defined by a triplet of keypoints, including a point on the midrib (M), a point on the stem (S), and a point near the leaf collar (C), and the relationships between those three keypoints. We implemented an anchor-free model to detect the distinct regions of leaf collars and to identify the points of interest for quantifying leaf angles. The approach bypasses the challenges faced by individual leaf detection and segmentation in field-based images. The specific objectives were to (1) implement a customized stereo-vision-based plant phenotyping platform to image maize plant canopy at different heights in the field; (2) develop an automated image processing pipeline to detect the regions and keypoints of interest and characterize plant architecture via a 3D modeling process and derive two important traits: leaf angle and its associated node height; (3) evaluate the performance of the proposed approach by comparing system-derived measurements with ground truth; and (4) explore the effectiveness of the newly developed system for characterizing leaf angle variations in different maize inbred lines in the field.

2 | METHODS

2.1 | PhenoBot 3.0 and PhenoStereo

PhenoBot 3.0 (Gai, 2020; Tuel, 2019) (Figure 1a) was used as the robotic ground-based sensor platform for data acquisition. The platform is designed for field-based plant phenotyping, especially for tall-growing plants such as maize and sorghum. With a unique narrow body design (0.508-m width) and a centrally articulated steering mechanism, PhenoBot 3.0 is able to navigate between crop rows with 0.76-m spacing (Gai et al., 2021). A sensor mast with adjustable height (between 2.1 and 3.7 m) is mounted on the vehicle to support an RTK-GPS module and images sensors. To avoid collision with the crop rows and keep a workable camera-to-object distance, the roll angle of the sensor mast was actively controlled to maintain the mast gravitationally vertical in the presence of uneven ground surfaces. The self-balanced sensor mast enables the phenotyping platform to image plant sections at different heights to cover the whole canopy. With the sensor mast and the image sensor configuration, PhenoBot 3.0 is capable of capturing various organ-level phenotypic traits located at different heights of maize plant canopy, such as leaf angle, stem diameter, ear height, tassel size, and so on.

PhenoStereo (Xiang et al., 2020) camera was used to acquire stereo imagery of maize plants in the field (Figure 1b). The custom-built stereo camera module houses two industrial color cameras equipped with a lens of 4.0 mm focal length. To overcome the variable outdoor lighting conditions, the module integrates an embedded computer and a high-intensity strobe lighting system for high-speed stereoscopic image capturing at a rate up to 14 frames per second (FPS). In all experiments, the aperture of the lens and the

1556467, 0, Downloaded from https://onlinelibrary.wiley.com/doi/10.1002/rob.22166, Wiley Online Library on [01/07/2023]. See the Terms and Conditions (https://onlinelibrary.wiley.com/terms-and-conditions) on Wiley Online Library for rules of use; OA articles are governed by the applicable Creative Commons Licenses



FIGURE 1 PhenoBot 3.0 and PhenoStereo. (a) PhenoBot 3.0 with a self-balanced sensor mast. PhenoStereo cameras were mounted at four different heights to capture side-view images of maize plants. (b) PhenoStereo with a self-contained embedded design and integrated strobe lights. [Color figure can be viewed at wileyonlinelibrary.com]

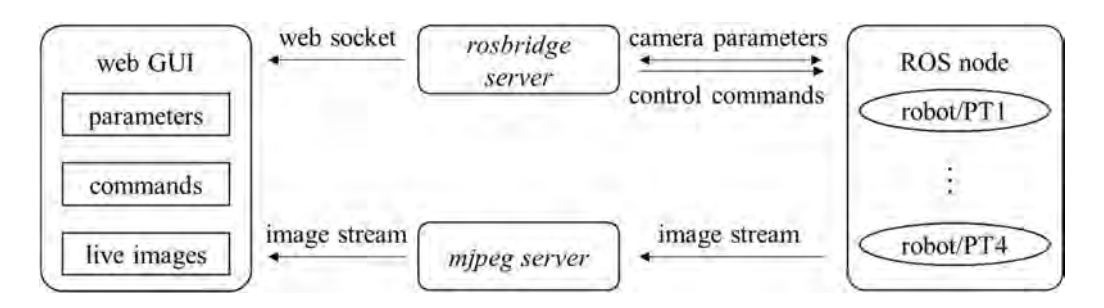


FIGURE 2 Overview of the software architecture.

strobe time were kept fixed at f/11 and 0.0015 s, respectively. PhenoBot 3.0 was equipped with four tiers of PhenoStereo cameras to capture side-view and close-range stereo images of maize plants in the field (Figure 1a). The four cameras used in this study (from bottom to top) were referred to as PT1-PT4. One camera (PT4) was mounted on the sensor mast to photograph the canopy near the maize tassel, and the other three were mounted on a customized frame in the back of the vehicle. Given the 0.76-m row spacing and the camera specifications, the system configuration resulted in a coverage of 2.22 m of the canopy in the vertical direction.

The software control system (Figure 2) was implemented in robot operation system (ROS) (Stanford Artificial Intelligence Laboratory et al., 2018). Each PhenoStereo camera was a ROS node, and a roscore node was run on the computer enclosed in PT1. A graphic user interface (GUI) based on Robot Web Tools (Toris et al., 2015) was developed to serve inputs and outputs. During data collection, the camera parameters and control commands were sent through the GUI and interacted with the ROS nodes wirelessly through the rosbridge protocol (Crick et al., 2017). In addition, the image stream was published by the

ROS nodes and displayed on the GUI through the *mjpeg server* to adjust camera parameters and preview images.

2.2 | Data acquisition

The field image acquisition was carried out at two test sites with different environmental conditions and multiple maize inbred lines. The data sets for system validation including (1) PS-Boone: PhenoBot acquired with four sets of PhenoStereo cameras at the Agricultural Engineering and Agronomy Research Farm of Iowa State University; and (2) PS-Ames: PhenoBot acquired with three sets of PhenoStereo cameras at the Curtiss Farm of Iowa State University. A summary of the data acquisition details is presented in Table 1. Two inbred lines, B73 (Russell, 1972) and Mo17 (Zuber, 1973), were used to investigate leaf angle architecture, and the remaining lines were randomly selected and used for system validation. Imagery data were collected on sunny days without the use of a shading structure. The mounting positions of PhenoStereo cameras were adjusted to cover the entire canopy. During data collection, Phenobot 3.0 navigated between the crop rows with the PhenoStereo cameras capturing side-view images of plants (Figure 3a). The shutter speed was set to 0.0003 s to avoid motion blur induced by robot motion, wind, and robot vibration. Images at different heights were collected and crossregistered to cover the entire canopy (Figure 3b-e).

We measured the angle between the midrib of a leaf and the stem segment below the leaf collar (Figure 4a); the supplementary angle of the measured angle served as the leaf angle. The associated node height of a leaf angle was defined as the vertical distance from the ground to the leaf collar. Two types of ground-truth data for leaf

TABLE 1 The characteristics of the two data sets used for system validation.

| Data set | PS4-Boone | PS3-Ames |
|---------------------------|--------------------------------|----------------------------------|
| Location | Agronomy Farm, Boone, IA | Curtiss Farm, Ames, IA |
| Days after planting | 97 | 73 |
| Operation time | 1-3 p.m., August 5, 2020 | 10-11 a.m., August 6, 2021 |
| Crop row spacing | 0.76 m | 3.35 m |
| Number of plants measured | 10 | 6 |
| Leaf angle range | 15-50° | 5-60° |
| Node height range | 0.3-2.0 m | 0.2-1.6 m |
| Camera-to-object distance | 0.38-0.51 m | 0.51-0.64 m |
| Frame rate | 5 FPS | 10 FPS |
| Driving speed | ~1 m/s | ~2 m/s |
| Weather conditions | Bright sunlight, light wind | Light sunlight, moderate wind |

angle were collected from manual measurements in the field and the reconstructed 3D models, respectively. For field measurements, leaf angles were measured using a protractor with its origin placed on the leaf collar (Figure 4a). To measure leaf angles from 3D models, a program was developed in which a user clicks four points (A, B, C, and D) on the point cloud to identify the direction of the stem and the leaf (Figure 4b). Node height ground-truth data were obtained using a tape measure in the field.

2.3 | Image processing

We developed a unique image processing pipeline named AngleNet for leaf angle detection and characterization (Figure 5). A novel presentation of maize leaf angle was proposed as a triplet of three keypoints, including a point on the midrib (M), a point on the stem (S), and a point near the leaf collar (C). As shown in Figure 5, each leaf angle is defined by three keypoints connected by two line segments. This pipeline consists of three major steps. First, a CNN-based model is trained to detect regions around leaf collars (Figure 5a) and three keypoints in each region (Figure 5b). The model detects an object as a center point and regresses other properties (e.g., width, height, offset) of the object at the center point. By eliminating the predefined set of anchor boxes, the model runs in an anchor-free manner and thereby is more efficient than bounding-box-based detectors. The two line segments (CS and CM) formed by the three keypoints play an important role in the leaf angle extraction step. The detection is performed on the right image. To improve the computational efficiency, a cropped image pair derived from left and right images based on the detected region of interest (RoI) is then used for stereo matching, and a disparity map is generated for 3D reconstruction (Figure 5c). The coordinate system is defined as follows: the x-axis is parallel to the robotic vehicle's heading direction, the y-axis is the vertical direction of plant growth, and the z-axis is perpendicular to the x-y plane pointing towards the plants. In this study, (x, y)represents the 2D image point coordinates in pixels, and (x, y, z) represents the 3D coordinates of a 2D point. To include the detected bounding boxes and ensure overlap between the left and right images, the cropped region for the image pair is centered at (x, y) with 2^*W width and 2^*H height, where (x, y) is the center of the bounding box detected in the right image, W and H are the width and height of the bounding box, respectively. Finally, the detection results in the 2D images are reprojected onto their 3D coordinates based on stereo camera calibration, and the random sample consensus (RANSAC) algorithm is used to fit two 3D lines to quantify the leaf angle (Figure 5d). At the same time, the node height is calculated based on the y coordinate of the leaf collar.

2.3.1 | Keypoint triplets for leaf angle detection

An angle in 2D or 3D can be specified by a triplet of points and their topology. For leaf angle measurements, the triplet includes a point

5564967, 0, Downloaded from https://onlinelibrary.wiley.com/doi/10.1002/rob.22166, Wiley Online Library on [01/07/2023]. See the Terms and Conditions (https://onlinelibrary.wiley.com/terms-and-conditions) on Wiley Online Library for rules of use; OA articles are governed by the applicable Creative Commons Licenses

Data collection and visualization. (a) PhenoBot 3.0 with the four-level stereo imaging configuration traversing between crop rows with 0.76-m spacing to capture side-view images. (b-e) The plant canopy imaged at different heights. Point clouds (b), (c), (d), and (e) are reconstructed 3D models from PT1, PT2, PT3, and PT4, respectively. [Color figure can be viewed at wileyonlinelibrary.com]

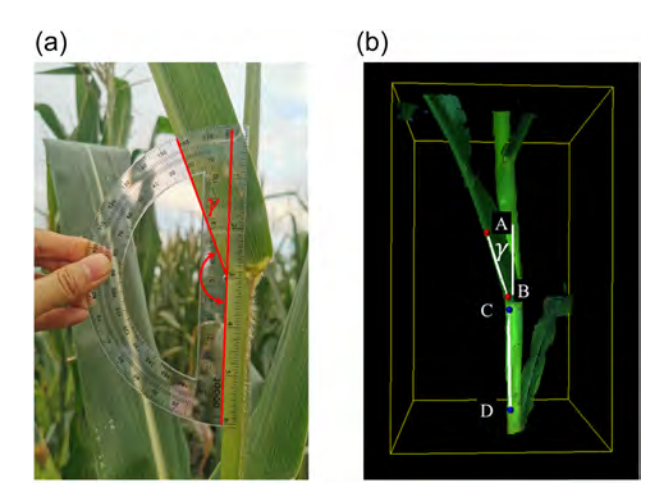


FIGURE 4 Two types of ground-truth data collection of leaf angle (y). (a) The angle between the midrib and the stem was measured using a protractor and the supplementary angle of the measured angle served as the ground truth. (b) The angle of the AB line and the extended DC line served as the ground truth when manually clicking four points in the 3D point cloud. [Color figure can be viewed at wileyonlinelibrary.com]

near the leaf collar (C), a point on the midrib (M), and a point on the stem (S). In this study, we aimed to identify the three keypoints with predefined relationships of a leaf angle in 2D images and reproject them into the 3D space to quantify the actual leaf angle. The region near a leaf collar, where a leaf intersects with a stem, has a unique appearance and provides a well-defined condition for the detection of keypoint C. However, defining keypoints S and M can be ambiguous because many homogeneous points along the direction of the midrib can be used to define a leaf angle. To solve this problem, we used a bounding box centered at the leaf collar to define the RoI (Figure 6). The width/length of the bounding box is around 350 pixels. Within each bounding box, the point on the centerline of the midrib and close to the border of the bounding box was defined as M (Figure 6). Similarly, the keypoint S was on the stem centerline and near the border of the bounding box. In AngleNet, an Rol near each leaf collar was first detected as a bounding box (Figure 5a). Subsequently, the locations of keypoints M and S became well-defined with respect to the collar and the boundary, and the triplet in the region inside the object bounding box could then be identified (Figure 5b).

15564967, 0, Downloaded from https://onlinelibrary.wiley.com/doi/10.1002/rob.22166, Wiley Online Library on [01/07/2023]. See the Terms and Conditions (https://onlinelibrary.wiley.com/terms-and-conditions) on Wiley Online Library for rules of use; OA articles are governed by the applicable Creative Commons Licensea

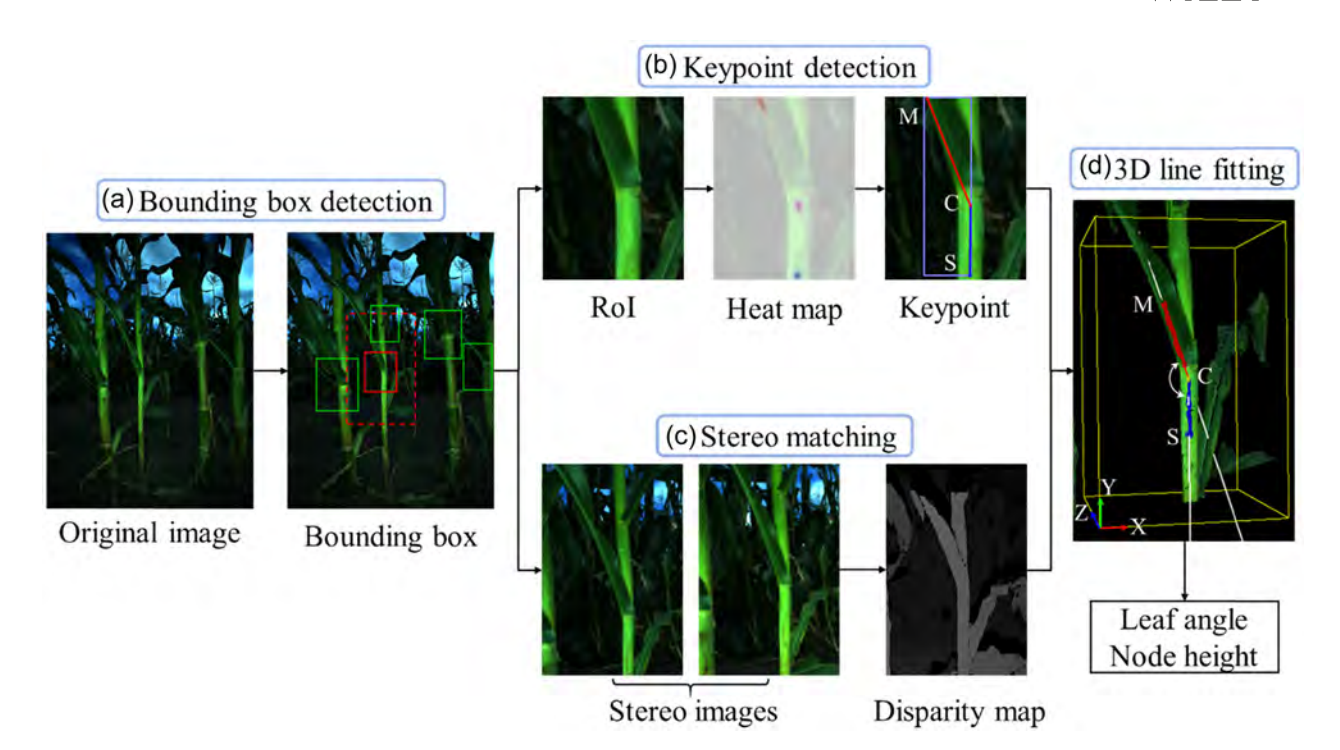


FIGURE 5 Automated image processing workflow of AngleNet for the characterization of 3D leaf angle. (a) Detection of Rols denotated by solid bounding boxes. The red solid bounding box is used as an example to illustrate the sequential processing steps. The red dashed bounding box is the expanded area used for stereo matching. (b) Keypoint detection. Three keypoints are extracted from the heat map of the Rol: a point near the leaf collar (C), a point on the midrib (M), and a point on the stem (S). (c) Stereo matching is carried out on the cropped stereoscopic images, and a disparity map is generated. (d) A 3D model reconstructed from the disparity map and color images. The detection results in 2D images were back-projected to the 3D space, and two lines (white) were fitted to compute the actual leaf angle. The supplementary angle of \angle MCS was defined as the leaf angle in this study. The pipeline outputs two types of architecture-related traits: leaf angle and its associated node height. [Color figure can be viewed at wileyonlinelibrary.com]



FIGURE 6 Schematic of the workflow of image annotation. The regions near leaf collars were first annotated by bounding boxes. Within each box, three keypoints (M, C, S) were identified for leaf angle characterization. The keypoint C is the intersection of the stem centerline and leaf midrib centerline. The point on the midrib centerline but near the border of the bounding box was annotated as the keypoint M. The same principle was used for the annotation of keypoint S. [Color figure can be viewed at wileyonlinelibrary.com]

Anchor-based detectors, such as Faster R-CNN (Ren et al., 2017) and YOLOv3 (Redmon & Farhadi, 2018), enumerate a nearly exhaustive set of anchor boxes and classify each of them, which can be inefficient and computationally complex. To overcome the drawbacks of anchor-based approaches, various anchor-free detectors that model an object as points instead of using a bounding box have been developed (Kong et al., 2020; Law & Deng, 2018). We

employed an anchor-free detector to detect the regions and keypoints of interest for leaf angle characterization. The detector represented each instance based on its features at the center point, and the height and width of the object were regressed at the center point without the predesigned set of anchors. The results were obtained using a modified CenterNet (Zhou et al., 2019) architecture. The region near a leaf collar was modeled as a single point located at

 $p = (\frac{x_1 + x_2}{2}, \frac{y_1 + y_2}{2})$, where (x_1, y_1) and (x_2, y_2) are the top left and bottom right points of the bounding box of the region, respectively. The detection of the object center is then transformed into a keypoint detection problem. In this study, the model takes an image of size $W \times H$ as input and aims to produce a $\frac{W}{R} \times \frac{H}{R}$ heatmap that represents the probability of leaf collar centers. Here, R represents the output stride and is set as 4 in this study. For the ground truth of heatmap, the values at object center are set to 1 and the other negative samples are set as 0. A single network is used to predict the keypoints \hat{Y} , offsets \hat{O} , and size \hat{S} . To train a network, each center point of object k is rendered by a Gaussian-shaped peak Y_{xy} and trained with focal loss L_k (Equation 1). The local maximums in the heatmap are the estimated centers, and height and width are predicted based on the images at each center. In addition, a local offset loss L_{off} (Equation 2) is trained to recover the discretization error caused by the resampling process. Finally, the object size regressed from the center point is trained with an L_1 loss L_{size} (Equation 3). The overall loss is the weighted sum of three loss terms: focal loss (L_k) , local offset loss (L_{off}) , and size loss (L_{size}). The prediction of the leaf angle triplets is also a keypoint estimation process. For an input image of size $W \times H$, the model outputs $\frac{W}{R} \times \frac{H}{R} \times 3$ heatmaps to predict the three keypoints (C, S, and M) that form the leaf angle. The locations of the three keypoints are regressed as offsets from the center. The ground-truth keypoint heat maps are trained with focal loss and local offset loss via a process analogous to that used for center detection.

$$L_{k} = \frac{-1}{N} \sum_{xy} \begin{cases} (1 - \hat{Y}_{xy})^{\alpha} \log(\hat{Y}_{xy}) & \text{if} \quad Y_{xy} = 1\\ (1 - Y_{xy})^{\beta}(\hat{Y}_{xy})^{\alpha} \log(1 - \hat{Y}_{xy}) & \text{otherwise} \end{cases}$$
 (1)

$$L_{\text{off}} = \frac{1}{N} \sum_{p} \left| \hat{O}_{\tilde{p}} - \left(\frac{p}{R} - \tilde{p} \right) \right|, \tag{2}$$

$$L_{\text{size}} = \frac{1}{N} \sum_{k=1}^{N} |\hat{S}_{p_k} - S_k|, \tag{3}$$

where α and β are hyper-parameters, N is the number of keypoints, and R is the output stride size. Two backbone networks were tested for this model: deep layer aggregation (DLA-34) (Yu et al., 2017; Zhou et al., 2019) and stacked hourglass network (HG-104) (Law & Deng, 2018; Newell et al., 2016). DLA-34 is an image classification network that implements deep layer aggregation structures to better fuse feature hierarchy across layers. The aggregation architecture employs hierarchical and iterative skip connections to encompass and extend densely connected networks and feature pyramid network. HG-104 is a fully convolutional neural network that consists of two sequential hourglass modules, each containing symmetric downsample and up-sample CNN layers with skip connections; originally used for human pose estimation (Newell et al., 2016). With a bottomup, top-down structure, the network can capture information across all scales of the image and consolidate the various relationship associated with the leaf collar (Figure 7). HG-104 has achieved stateof-the-art performance on other keypoint detection tasks (Wei et al., 2020; Y. Zhang et al., 2018).

Two different data sets with rectified stereo images were annotated for training and testing. In the first data set, 620 images were manually labeled with a bounding box around each leaf collar. The second data set contained 240 images, in which each leaf angle was marked with a triplet of three dots. The annotated images were randomly split into training, validation, and test data sets at a ratio of 7:2:1. To further increase the diversity of the input images and the robustness of the network, we applied image augmentation techniques including randomly flip 50% of the images, randomly

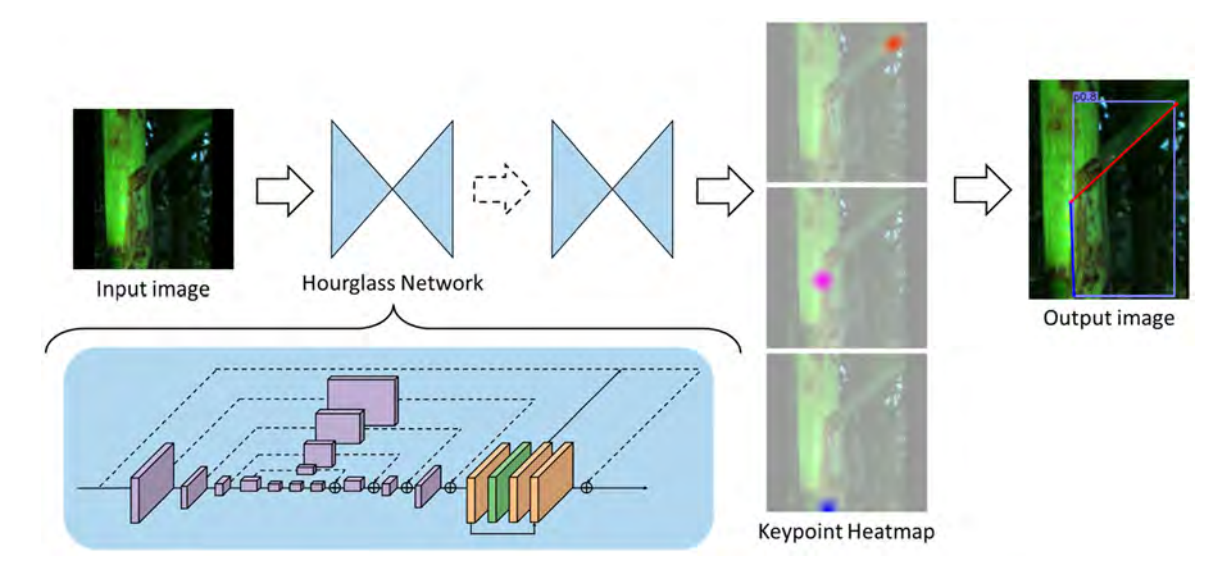


FIGURE 7 Illustration of our keypoint detection framework with hourglass backbone. Each hourglass module contains down-sample and upsample layers to capture and consolidate information. The network takes an image as input and produces probability heatmaps for each keypoint. The final triplet estimate provided by the max activations across each heatmap is shown on the right. [Color figure can be viewed at wileyonlinelibrary.com]

scaling (between 0.8 and 1.2), and horizontal/vertical shifting (between 0.9 and 1.1). The Adam optimizer (Kingma & Ba, 2014) was used to minimize the loss function of AngleNet. The trained models that achieved the best performance on the test data set were used for leaf angle characterization. AngleNet was implemented with PyTorch (Paszke et al., 2017). A high-performance workstation with a NVIDIA Titan Xp GPU, a 2.2-GHz Xeon Gold 5120 CPU, and 32 GB RAM were used to train the models.

2.3.2 | 3D reconstruction of the canopy

Measuring leaf angle from 2D images can be inaccurate due to variable leaf poses relative to the camera. Therefore, the 3D models of the canopy were reconstructed for leaf angle measurement. The 3D reconstruction process involves four steps: calibration, rectification, stereo matching, and triangulation. Stereo matching is particularly crucial for reconstructing a dense 3D canopy model. In the first step, each stereo camera is calibrated with a checkerboard pattern to obtain the intrinsic parameters (e.g., focal length, pixel size, principal point, baseline, and distortion coefficients) and extrinsic parameters (e.g., camera pose). The lens distortion is then removed and the stereoscopic image pair is rectified using the intrinsic parameters so that the two image planes are row-aligned. Subsequently, stereo matching takes the rectified image pair as input and computes a disparity map by finding corresponding points between the left and right images. The disparities are inversely proportional to the depth values (Figure 5c). Finally, the process of triangulation back-projects the disparity map to 3D coordinates to generate a point cloud (Figure 5d). Here, the background in the reconstructed point cloud was removed by filtering out points with depth values greater than 0.8 m.

Stereo matching is a photogrammetric technique that reconstructs depth information based on a stereoscopic image pair (Mehltretter & Heipke, 2021). Compared with structure from motion (SfM), a commonly used 3D reconstruction technique in photogrammetry, two-view stereo imaging requires a minimum number of input images, which makes it practical for in-field applications. Many traditional algorithms, such as semiglobal matching (Hirschmüller, 2008), have been developed to detect stereo correspondence. However, stereo matching for field crops can still be challenging due to low-texture surfaces, heavy occlusions, and variable lighting conditions. Recent breakthroughs in machine learning and deep learning techniques have achieved impressive results in stereo correspondence matching (Poggi et al., 2020). One of the most impactful works in this area describes MC-CNN (Zbontar & Lecun, 2016), a CNN-trained algorithm to robustly predict the similarity of two image patches. In the current study, we used a stateof-the-art stereo-matching method known as 3D-MST (Li et al., 2017) to compute disparity images for the input stereo pairs and reconstruct the dense canopy. This algorithm uses MC-CNN for matching cost computation and features a cost-aggregation method with minimum spinning tree (MST)-based support region filtering. A

multi-MST structure was developed to reduce the computational complexity, and a PatchMatch random search strategy was implemented to efficiently find the 3D labels of each pixel. A 3D-MST is one of the top-ranking algorithms in the Middlebury 3.0 benchmark (https://vision.middlebury.edu/stereo/) and has generated convincing results for reconstructing dense plant canopies in the field (Bao, Tang, Breitzman, et al., 2019).

2.3.3 | Trait extraction

Two- to three-dimensional reprojection

Through keypoint detection, a triplet of points (C, M, and S) and two edges (CM and CS) were created for each leaf angle (Figure 5b). These detection results were reprojected into the 3D point cloud using the intrinsic parameters of the stereo camera (Figure 5d). After reprojection, the 3D positions of the targets were represented in the left camera's rectified coordinate system, where the origin is located at the projection center of the left camera and the y-axis represents the direction perpendicular to the ground plane pointing upward.

Estimation of leaf angle

Ideally, the 3D coordinates of the three keypoints can be used for angle measurement. However, there are some cases related to the absence of depth measurements or problematic depth measurement with large errors in some pixels. To increase the robustness of measuring an angle, the two edges (CM and CS) formed by the three keypoints were used to estimate leaf angle. Co-registration of color and 3D images provides the 3D locations of the two edges. However, projecting a line segment to a point cloud results in a dimensionality increment, an operation that does not generally result in a unique 3D line. In addition, it is possible that some remaining noise might be present in the resulting 3D patch in the point cloud. Such noise points can arise from curved leaf blades, occlusions, or stereo-matching errors. To robustly determine the 3D locations of the CM and CS edges, the RANSAC algorithm (Fischler & Bolles, 1981) was implemented to fit lines in the 3D space. The algorithm iteratively fits a line based on two randomly selected points. The line fit with the most inliers is regarded as the final fit. For each edge, the RANSAC line fitting algorithm takes all the candidate points in the 3D patch (the red/blue points in Figure 5d) as input and outputs a position vector \mathbf{p} and a direction vector \mathbf{d} that determine a line.

The RANSAC-based line fitting algorithm can deal with a moderate amount of noise in the point cloud. However, we observed that when a 2D line was reprojected onto a curved leaf blade, the corresponding 3D patch tended to be discontinuous in the 3D space. In this case, the fitted line generated by the RANSAC algorithm did not effectively represent the direction of the midrib. To solve this problem, a fitting score was defined to remove these lines. The fitting score was defined as the ratio of the inliers to the total number of input points, where point pt was regarded as an inlier if its distance (Equation 4) to the detected line was <0.005 m. An edge was regarded as valid for a leaf angle measurement if the fitting score was

larger than 0.8; otherwise, the fit and the corresponding 3D patch were rejected from further analysis. Finally, the direction vectors of two valid edges were used to estimate leaf angle (Equation 5).

$$dis = \frac{\|d \times (p - pt)\|}{\|d\|}, \tag{4}$$

$$\alpha = \frac{\arccos\left(\left|\frac{d_5 \cdot d_m}{\|d_5\| \|d_m\|}\right|\right)}{\pi} *180^\circ, \tag{5}$$

where d_s and d_m are the direction vectors of CM and CS in the 3D space, respectively, ||v|| is the Euclidean norm of the vector v, |x| is the absolute value of x, and α is the leaf angle.

Estimation of node height

Node height is defined as the distance in the vertical direction between the leaf collar and the ground plane. In this study, the y coordinate of the detected keypoint C was used to calculate node height. However, the corresponding y coordinates of point C in the 3D point cloud are based on the local coordinate system of each stereo camera. To generate comparable node height values, the node height was estimated by adding the vertical distance between the camera and the ground to the y coordinates of point C.

2.4 | Accuracy assessment

The performance of the newly developed algorithm was evaluated in terms of its accuracy in accomplishing two critical steps: the detection of leaf collars in 2D images, and the estimation of leaf angle and node height in 3D point clouds.

2.4.1 Detection accuracy assessment

The performance of the AngleNet model in bounding-box detection was evaluated by average precision (AP) (Equation 6). In addition, intersection over union (IoU, Equation 7) was used as an indicator of position and shape accuracy. IoU is defined as the ratio of intersection area over the union area of the predicted value and ground truth.

$$AP = \sum_{k=0}^{k=n-1} [Recall(k) - Recalls(k+1)] * Precisions(k) Recall(n)$$

$$= 0, Precisions(n) = 1$$
(6)

$$loU = \frac{Area of Overlap}{Area of Union} \times 100\%, \tag{7}$$

where n is the number of thresholds.

To evaluate the performance of keypoint detection, pixel error (PE) and normalized error (NE) were utilized. Pixel error (Equation 8) is defined as the Euclidean distance between the predicted point (x, y) and the ground truth $(x_{\rm gt}, y_{\rm gt})$. Normalized error (Equation 9) is

calculated as the PE value normalized by the length of the leaf angle skeleton.

PE =
$$\sqrt{(x - x_{gt})^2 + (y - y_{gt})^2}$$
 (8)

NE =
$$\frac{PE}{|CS| + |CM|} \times 100\%$$
, (9)

where |CS| and |CM| are the lengths of line segments CS and CM (Figure 5b), respectively, in pixels.

2.4.2 | Accuracy assessment of leaf angle and node height estimations

We investigated the accuracy of leaf angle measurements by comparing the AngleNet-derived values, ground truth measured in the field, and ground truth manually measured in the 3D point clouds, as described in Section 2.1.2. The node height was evaluated by comparing system-derived measurements to in-field manual measurements. The Pearson correlation coefficient (r, Equation 10), coefficient of determination (R^2 , Equation 11), and mean absolute error (MAE, Equation 12) were used as statistical metrics to evaluate the system performance in estimating leaf angle and node height.

$$r = \frac{\sum (x_i - \bar{x})(y_i - \bar{y})}{\sqrt{\sum (x_i - \bar{x})^2 \sum (y_i - \bar{y})^2}},$$
 (10)

$$R^2 = 1 - \frac{\sum (\hat{y}_i - \bar{y})^2}{\sum (y_i - \bar{y})^2},$$
 (11)

15564967, 0, Downloaded from https://onlinelibrary.wiley.com/doi/10.1002/rob.22166, Wiley Online Library on [01/07/2023]. See the Terms and Conditions (https://onlinelibrary.wiley.com/terms-and-conditions) on Wiley Online Library for rules of use; OA articles are governed by the applicable Creative Commons Licensea

MAE =
$$\frac{1}{n} \sum_{i=1}^{n} |x_i - y_i|$$
, (12)

where x_i and y_i denote actual values from manual measurements and estimated values measured by AngleNet, respectively. \bar{x} and \bar{y} represent the mean of the values. \hat{y}_i is the predicted value of y for observation i, and n is the total number of measurements.

3 | RESULTS

PhenoBot with multiple tiers of PhenoStereo cameras located at different heights was able to cover the entire maize canopy. Representative examples captured by the four camera sets (PT1-PT4) are shown in Figure 8. Overall, the AngleNet model successfully addressed various challenges in leaf angle measurement. AngleNet was robust to diverse leaf poses relative to the camera, which resulted in different viewing angles, including the (1) side view of the lower side of the leaf blade (Figure 8a, PT1); (2) side view of the upper side of the leaf blade (Figure 8a, PT2); (3) front view of the lower side of the leaf blade (Figure 8a, PT3); and (4) front view of the upper side of the leaf blade (Figure 8a, PT4). Among these viewing angles, (1) and (4) were optimal cases because the midrib was fully exposed to the camera and the leaf angle was located at a plane parallel to the image plane. PT2 posed a challenge for the detection

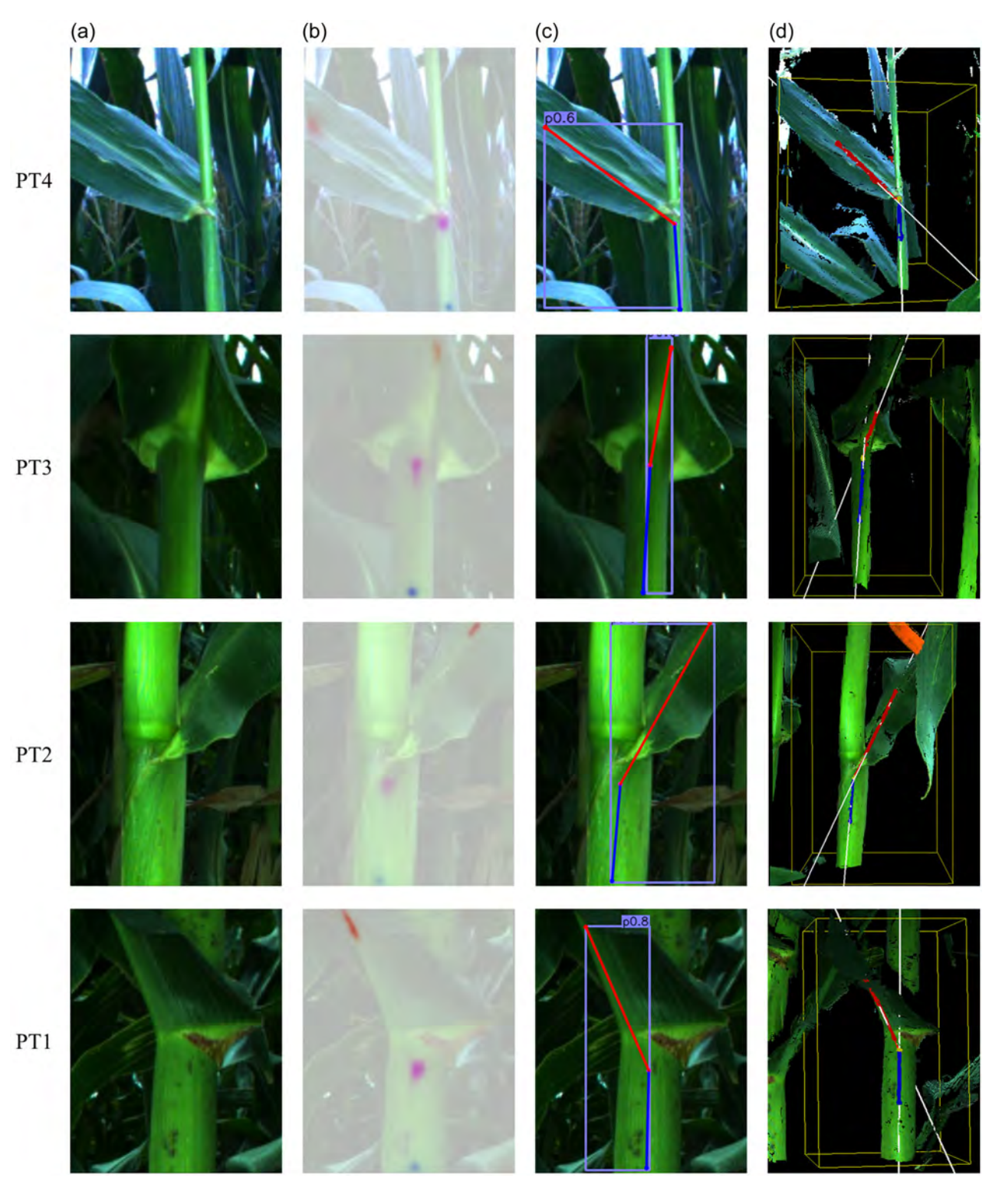


FIGURE 8 Typical examples of leaf angle measurements with intermediate results along the entire height of maize plants. (a) The Rols detected from original images, which were generated by the four camera heads at different heights. (b) Heat maps produced by the AngleNet model, representing the probability that each pixel represents the location of each keypoint. (c) Detection results extracted from the prediction heat map. The red and blue edges represent the directions of the midrib and stem, respectively. (d) Leaf angle measurements in 3D point cloud, where the white lines are fitted from the two detected edges in 3D space. [Color figure can be viewed at wileyonlinelibrary.com]

of keypoint M due to poor midrib visibility, while PT3 required an accurate 3D model for measuring the true leaf angle because the leaf pose was perpendicular to the image plane. The results illustrate that the trained CNN model could accurately detect RoIs and keypoints for leaf angles with various leaf orientations and under different illumination and occlusion conditions.

Figure 8d shows the qualitative results of 3D reconstruction and line fitting. Despite the background complexity and exposure differences, the stereo-matching algorithm effectively reconstructed 3D models of the maize canopy across different heights. In addition, 3D-MST performed quite well in handling leaf blades with a homogeneous appearance (color and texture), which allowed reconstructing accurate 3D models with smooth and continuous plant surfaces. This superior reconstruction quality provided a reliable 3D point distribution for RANSAC line fitting. The RANSAC-based algorithm robustly detected the line that represented the direction of a midrib/stem (Figure 8d). In addition, the algorithm was insensitive to the random noise introduced by the reprojection of a 2D line to a 3D patch.

3.1 | Detection performance

We evaluated the object detection performance of the AngleNet model at two stages. During the first stage, the Rol is localized by detecting a rectangular bounding box, and during the second stage, the triplet of keypoints is detected. Two different feature extraction backbones were tested, and the one with optimal performance was used for AngleNet. Figure 9 shows the Precision–Recall curves of the proposed model trained with DLA-34 and HG-104. The model trained with DLA-34 can produce more accurate predictions than HG-104, supported by a higher precision value at the same recall value and IoU threshold. However, the

Precision-Recall 1.0 0.9 0.8 recision 0.7 0.6 HG-104 AP= 0.908 @IoU = 0.5 HG 104 AP= 0.595 @loU = 0.7 0.5 DLA-34 AP= 0.843 @loU = 0.5 DLA-34 AP= 0.580 @IoU = 0.7 0.0 0.2 0.4 0.6 0.8 1.0

FIGURE 9 Precision-recall (PR) curves of models trained with DLA-34 and HG-104 in detecting leaf collars on the test data set with different IoU thresholds and corresponding AP values. An ideal PR curve should pass through the top-right corner (i.e., 100% for both precision and recall). [Color figure can be viewed at wileyonlinelibrary.com]

model trained with HG-104 can achieve higher maximum recall values, indicating the model has a higher ability to find all the relevant cases. Overall, the model trained with HG-104 backbone produced better results, as illustrated by the larger AP values both at $IoU_{(0.5)}$ and $IoU_{(0.7)}$. The trained model achieved an AP of 0.908 at $IoU_{(0.5)}$ on the test data set, highlighting the effectiveness of the model in detecting the RoI for leaf angle measurements. For the second stage, the detector with an HG-104 backbone successfully identified 279 of 282 angles, while the model trained with the DLA-34 backbone detected 263 samples. No false detections were produced by either model. Based on the detection rate, the HG-104 was used as the backbone model for keypoint detection in AngleNet.

To evaluate the localization accuracy, we calculated the mean and standard deviation (Table 2) for PE and NE described in Section 2.3.1. Overall, the deviations were less than 3% of the length of the leaf angle skeleton for all keypoints, indicating strong model robustness. Keypoint M produced higher PE and NE than the two other keypoints. The largest pixel errors for the three classes of keypoints in the test data set were mainly caused by occlusions (Figure 10). However, as shown in the examples in Figures 8 and 10, most deviations were along the direction

TABLE 2 Euclidean distance (in pixels) between the detected keypoints and ground truth normalized by the length of the leaf angle skeleton.

| | Pixel error (PE) | | Normalized error (NE, %) | |
|----------|------------------|-------|--------------------------|------|
| Keypoint | Mean | SD | Mean | SD |
| С | 6.55 | 5.18 | 1.78 | 1.29 |
| М | 10.41 | 10.08 | 2.93 | 3.19 |
| S | 5.52 | 4.45 | 1.52 | 1.26 |

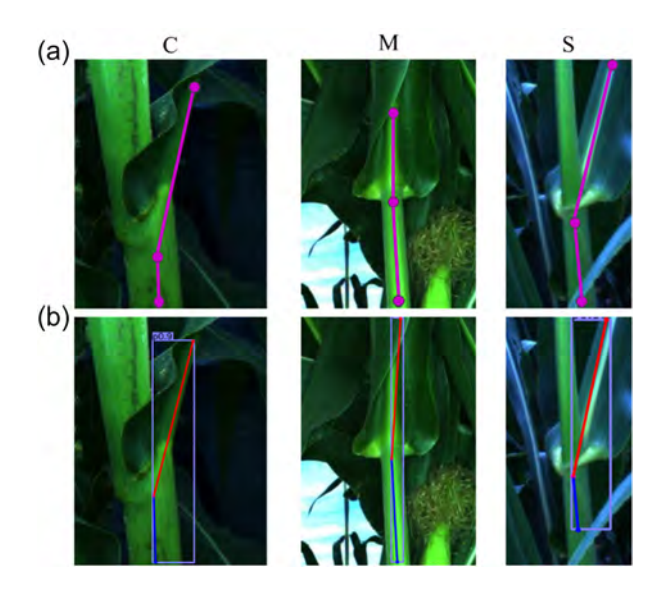


FIGURE 10 The largest pixel errors of keypoints C, M, and S in the test data set. (a) Manually labeled ground truth. (b) Keypoint detection results produced by AngleNet. [Color figure can be viewed at wileyonlinelibrary.com]

of the midrib/stem, which has minimal impact on angle measurement. To statistically evaluate the effectiveness of the keypoint predictions, we compared the angles estimated based on the detection results to the angles computed based on manually labeled keypoints. The mean and standard deviation of the angle errors were 1.94° and 1.67°, respectively.

3.2 | Accuracy of leaf angle estimates

The leaf angle estimates obtained using the proposed approach were highly correlated (r > 0.87, MAE < 5°) with in-field measurements

(Figure 11a,b). For both data sets, the intercept of the fit line was positive, indicating a general overestimation of leaf angles compared to the ground truth. The errors in leaf angle estimation were due to a number of factors, including keypoint location errors, inaccurate line fitting, and the inability to reconstruct an accurate 3D model. Another possible source of random error is errors in ground-truth collection. Compared with field-based ground truth, the estimated leaf angles had a stronger correlation with the references from the point cloud data (Figure 11c,d). Possible reasons for this include the following: (1) the second ground-truth collected from point cloud excludes the errors caused by 3D reconstruction; (2) due to the time interval between imaging and measuring, the leaf angle may have

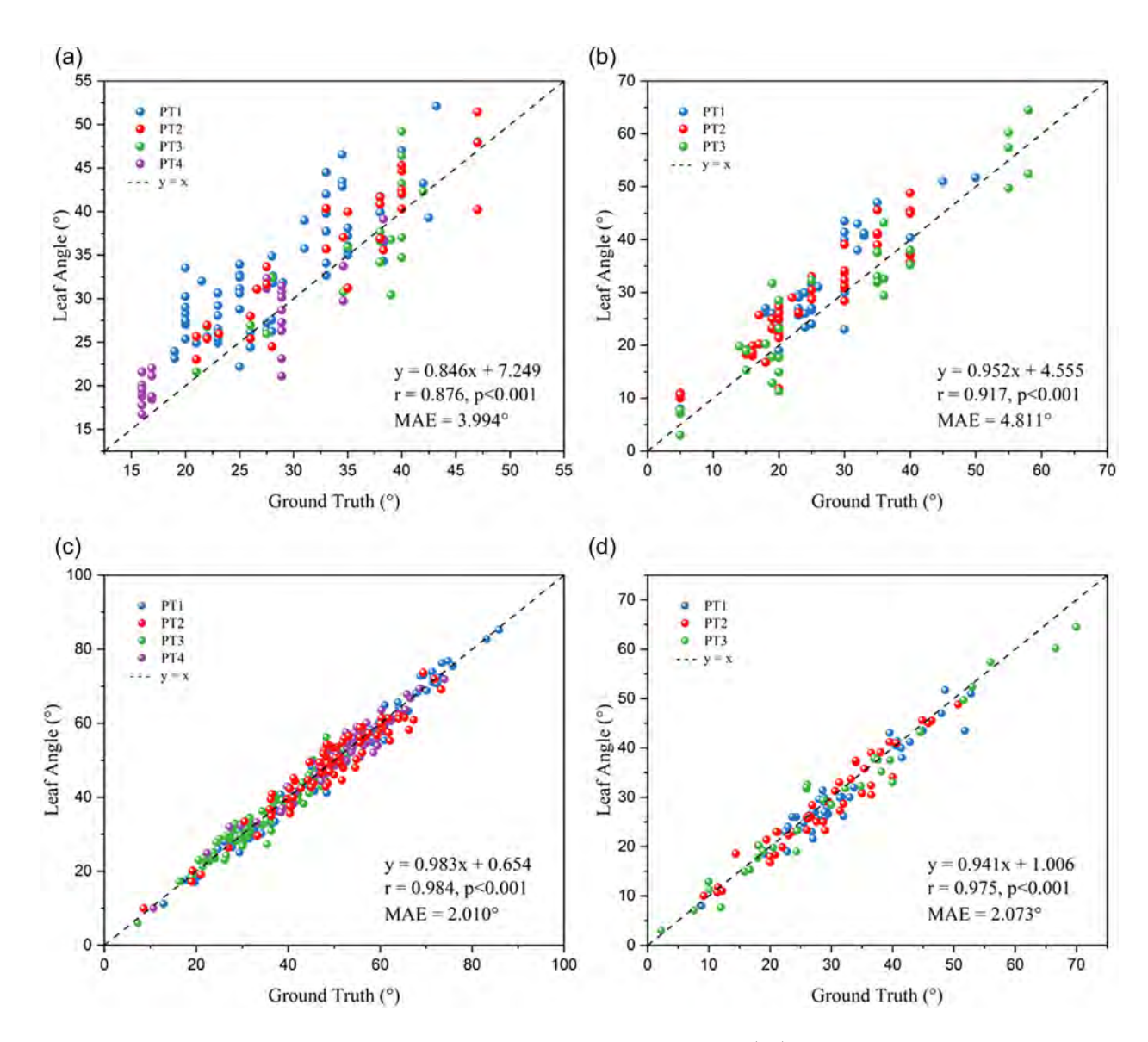


FIGURE 11 Comparison of AngleNet-derived leaf angles with reference measurements. (a,b) Comparison of estimated leaf angles with infield manual measurements collected using a protractor of PS4-Boone and OS3-Ames, respectively. (c,d) Comparison of estimated leaf angles with reference measurements manually measured from the 3D point clouds of PS4-Boone and PS3-Ames, respectively. [Color figure can be viewed at wileyonlinelibrary.com]

changed physically due to differences in wind and sunlight conditions, thereby affecting in-field ground-truth measurements; and (3) measuring leaf angles in the field using a protractor introduces more random errors than measuring leaf angles from a point cloud.

3.3 | Accuracy of node height values

Overall, the node heights calculated using the proposed approach were highly correlated (r > 0.99) with the manual measurements made in the field (Figure 12). The slope of the regression equation was close to 1, suggesting that system-derived node height values can be used as a direct estimate of the locations of leaf angles. We performed statistical analysis of the data collected by different camera heads (Tables 3 and 4), finding that the highest camera (PT4 in PS4-Boone and PT3 in PS3-Ames) had a significantly lower correlation coefficient than the other lower camera sets. The main reason for this difference is that the leaf collars imaged by the higher camera were located at relatively high positions, making it difficult to manually measure the node height in an accurate manner. Additionally, the top leaves of maize plants are less rigid than the bottom leaves, making them more sensitive to the movements caused by wind and PhenoBot. In general, all cameras in the two data sets achieved satisfactory performance, with a high correlation (r > 0.94) and a low mean absolute error (MAE < 4.2 cm). However, the model has a better performance in PS4-Boone than in PS3-Ames. Compared to PS4-Boone, the data collection in PS3-Ames has faster driving speed and longer camera-to-object distance, therefore produced stronger vibrations of the sensor mast and larger accumulated errors.

3.4 | Leaf angle distribution in B73 and Mo17

Finally, we used the AngleNet pipeline to explore the variations in leaf angle between two inbred maize lines: B73 and Mo17. To analyze the distribution of leaf angles throughout the canopy, we performed second-order polynomial fitting between leaf angle and the corresponding node height for each line (Figure 13). B73 exhibited erect leaves in the upper canopy and horizontal leaf angles in the lower canopy, which is consistent with a previous report (Dzievit et al., 2019). More specifically, the leaf angle of B73 had a negative relationship with node height. This configuration, with

TABLE 3 Comparison of the node height estimation accuracies of different camera heads for PS4-Boone.

| Camera | Linear fitting | r | MAE (cm) |
|--------|---------------------|-------|----------|
| PT1 | y = 0.928x + 2.243 | 0.992 | 1.581 |
| PT2 | y = 0.974x + 0.306 | 0.994 | 1.977 |
| PT3 | y = 0.963x + 1.041 | 0.991 | 2.269 |
| PT4 | y = 0.867x + 23.317 | 0.956 | 2.508 |

TABLE 4 Comparison of the node height estimation accuracies of different camera heads for PS3-Ames.

| Camera | Linear fitting | r | MAE (cm) |
|--------|--------------------|-------|----------|
| PT1 | y = 1.014x - 0.830 | 0.982 | 2.956 |
| PT2 | y = 0.938x + 6.009 | 0.971 | 3.485 |
| PT3 | y = 0.948x + 6.641 | 0.949 | 4.120 |

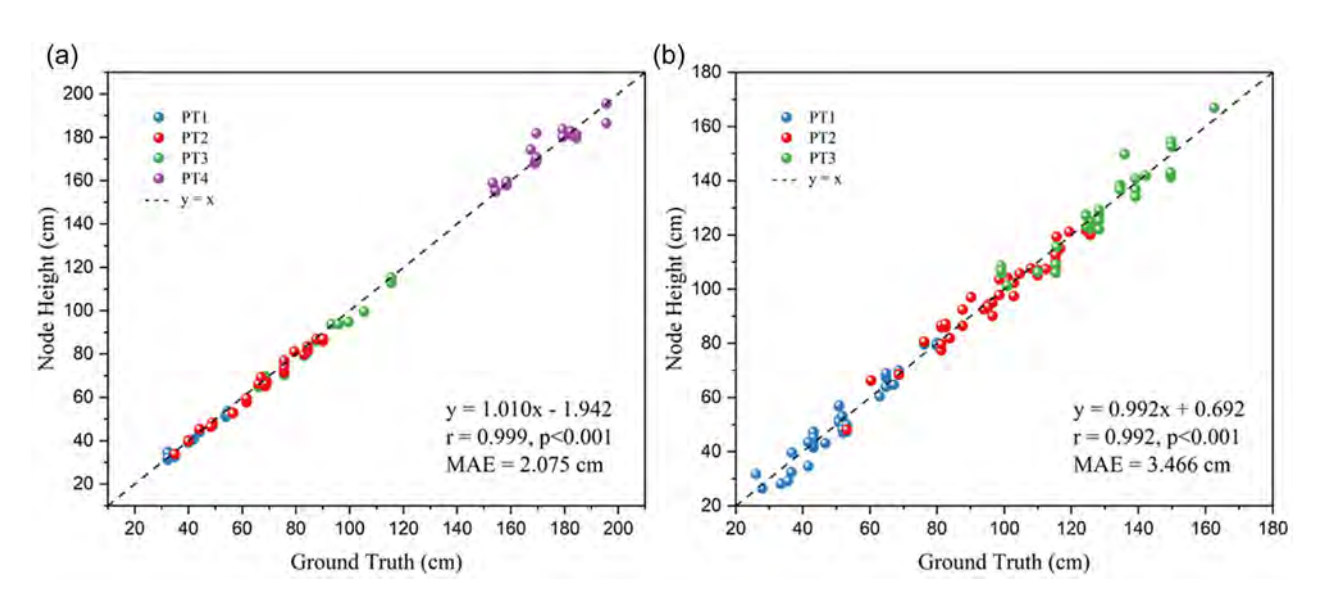


FIGURE 12 Comparison of AngleNet-derived node height values with ground truth. (a) Comparison of estimated node height with in-field manual measurements collected using a measuring tape of PS4-Boone. (b) Comparison of estimated node height with in-field manual measurements collected using a measuring tape of OS3-Ames. [Color figure can be viewed at wileyonlinelibrary.com]

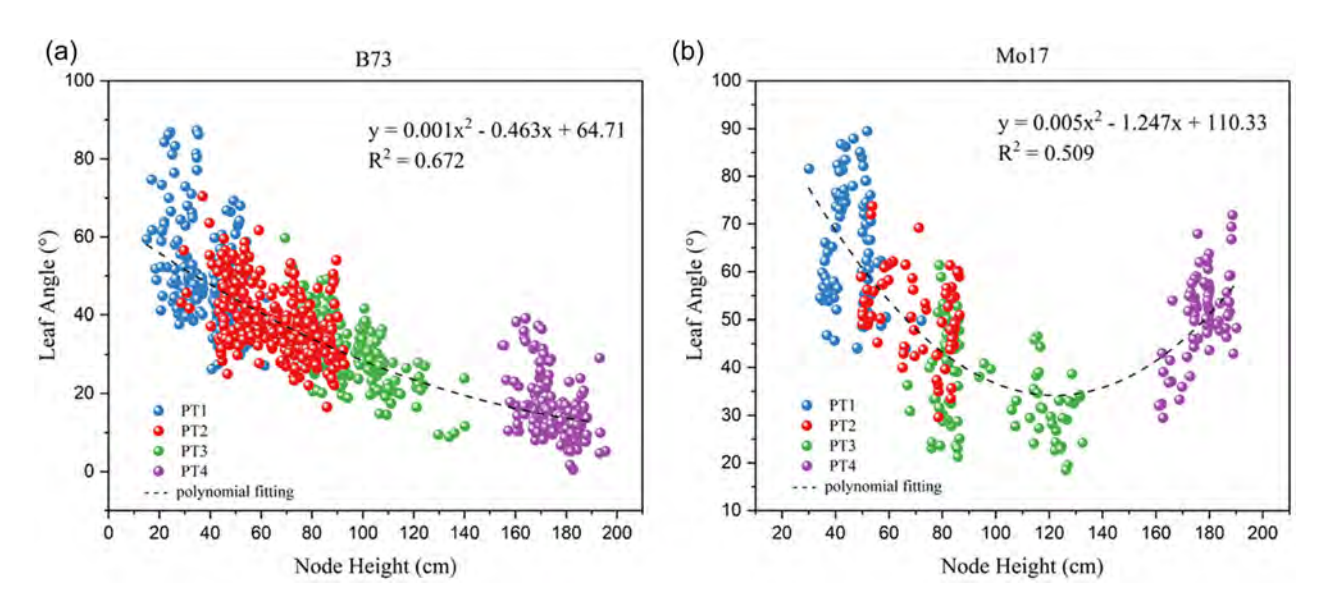


FIGURE 13 Leaf angle distribution along the entire height of B73 and Mo17 based on data generated by AngleNet. (a) The leaf angle of B73 decreased with increasing height. (b) The leaf angle of Mo17 initially decreased in the lower canopy and then increased in the upper canopy. [Color figure can be viewed at wileyonlinelibrary.com]

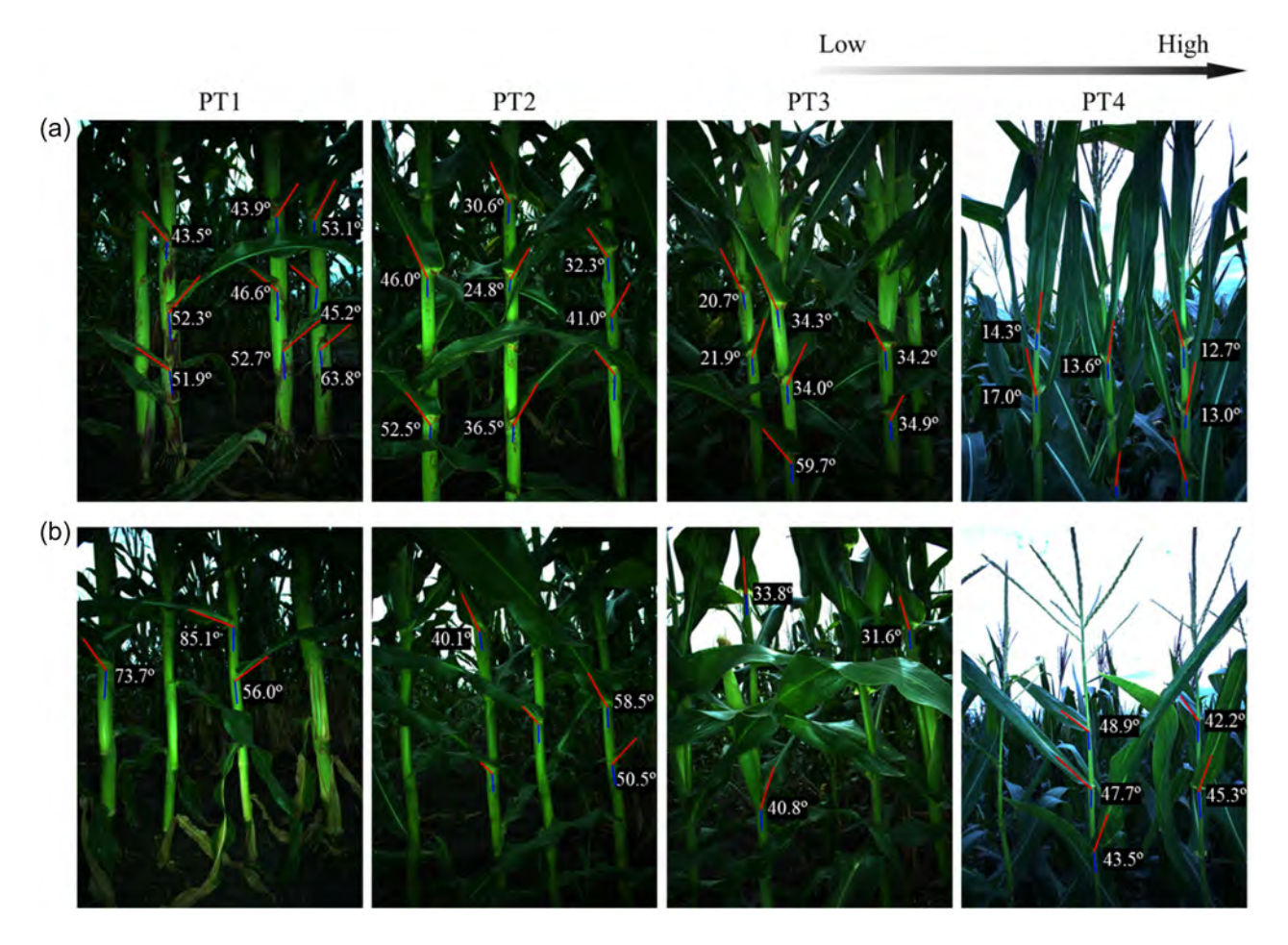


FIGURE 14 Sample outputs generated by the AngleNet pipeline showing comparisons of leaf angle at different heights between B73 and Mo17. The red and blue lines represent the directions of the midrib and stem, respectively; their supplementary angle was measured as the leaf angle. (a) B73 exhibited gradually decreasing angles starting from the bottom and had upright leaves at the top. (b) Mo17 had more horizontal leaf architecture throughout the canopy, with relatively erect architecture around ears. [Color figure can be viewed at wileyonlinelibrary.com]

increasingly upright leaves from the bottom to the top, maximizes the potential for light capture and increases the photosynthetic conversion efficiency (X. Zhang et al., 2017). Mo17 showed horizontal leaf angles near the top and bottom of the canopy but relatively erect architecture in the middle part of the canopy, especially around ears. As shown in the sample images captured by PT4 (Figure 14), the uppermost leaf angles of Mo17 were obviously larger than those of B73. Several angles were successfully detected in 2D images but failed to be measured in 3D space, primarily as a result of one of two situations: (1) the 2D edge was reprojected onto a wavy-shaped leaf blade and was rejected in 3D space because of a low fitting score; or (2) the angle was located near the boundary of one image and was absent from the other image of a stereo pair.

4 | DISCUSSION

The use of PhenoBot equipped with multiple tiers of PhenoStereo cameras provided an efficient and effective solution for high-resolution RGB and depth imaging of tall-growing crops in the field. The image acquisition process was conducted by manually driving the robotic vehicle between the crop rows at a walking speed. The time required for image acquisition is about 3–4 s for 20 plants per plot. For manual measurements, it takes about 8–10 min per plot to measure the leaf angle and the corresponding node height of four representative plants. With the automated image processing pipelines, the proposed approach in this study could effectively reduce the labor cost in leaf angle measurement.

Previous leaf angle-related research in maize has focused on single leaf or averaging the phenotypes from multiple leaves (X. Zhang et al., 2017; Zhao et al., 2018). However, it is important to phenotype leaves in different parts of the canopy to dissect the genetic control of leaf angle (Dzievit et al., 2019). Instead of

measuring a single plant or selected leaves, the proposed method measures the angle of all the nonoccluded leaves and provides the leaf angle distribution throughout the canopy for the whole population. Given that we have multiple plants within a plot, the approach could ensure the availability of leaf angles (the part with leaf midrib and stem) that are nonoccluded at a certain height level. Therefore, the proposed method can better reveal the canopy-wide leaf angle architecture compared to measuring selective plants.

One of the major limitations of the system is that expanded leaves occasionally blocked the view of the middle cameras due to narrow spacing and dense canopies. A possible solution to this problem is to increase the number of stereo cameras vertically. In this way, a leaf angle may be invisible to one camera but visible to another camera at a different height. Another alternative involves placing two camera sets with varying horizontal viewing angles at the same height, which could potentially mitigate the obstruction of camera views and the occlusions resulting from different plant orientations and leaf poses. Most sophisticated approaches used to extract leaf angles from 2D and 3D images involve segmenting and skeletonizing maize plants to analyze plant architecture (Cabrera-Bosquet et al., 2016; Das Choudhury et al., 2018; Wu et al., 2019, 2020; Zermas et al., 2020). For example, Bao, Tang, Srinivasan, et al. (2019) implemented a skeletonization-based algorithm to segment individual leaves and measure leaf traits based on leaf skeleton segments, an MAE of 2.8° and a coefficient of determination (R2) of 0.83 were achieved for leaf angle. Though high accuracies were obtained, the study was carried out for maize plants with increased row-spacing and inter-plant spacing to reduce occlusions caused by dense canopies. The previous methods reply on visible leaf tips for leaf segmentation (Gaillard et al., 2020; Souza et al., 2021) and need to adjust a set of parameters to achieve satisfactory performance (Bao, Tang, Srinivasan, et al., 2019; Wu et al., 2019; C. Zhu et al., 2020), which are not feasible for large-scale field-based

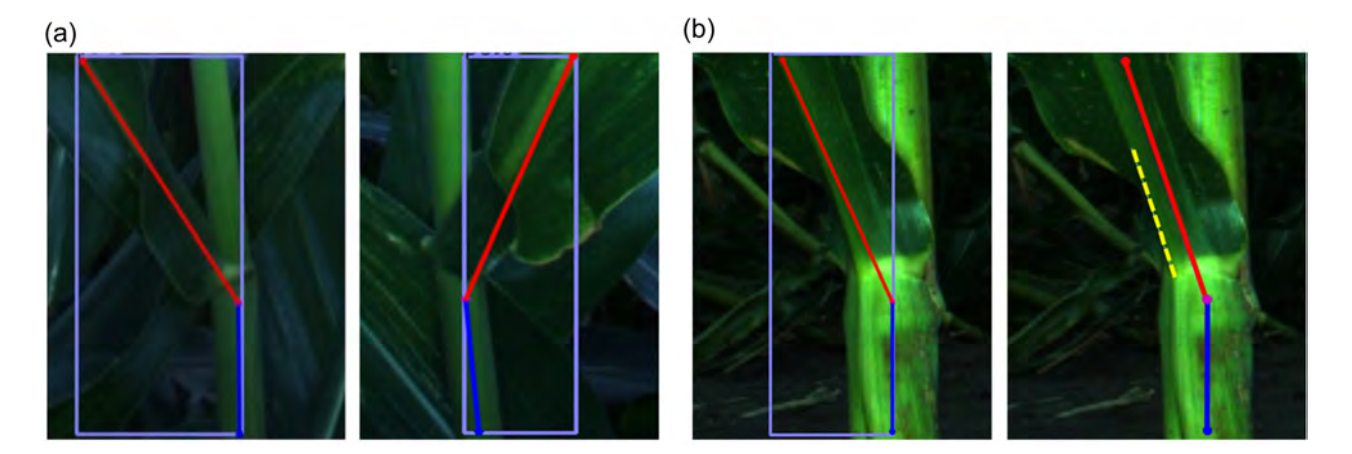


FIGURE 15 Limitations of AngleNet. (a) The midrib direction lines were located on a rolling leaf, where the resulting point cloud in 3D was not suitable for line fitting. (b) An alternative way to refine leaf angle topology in a 2D image. Left: the initial detection results produced by AngleNet. The red line is not exactly parallel to the direction of the midrib. Right: the direction of the midrib was refined based on a local edge (yellow dashed line). [Color figure can be viewed at wileyonlinelibrary.com]

XIANG ET AL. 17

applications due to the space resolution of the raw data and occlusion of nearby plants. The AngleNet pipeline proposed in this study focuses on the regions near leaf collars, which bypasses the complex procedures of individual plant and leaf segmentation. The leaf angle is located based on its associated height. Inspired by human pose estimation, this is the first study to implement the topology of keypoints for leaf angle measurement. The AngleNet pipeline showed the ability to quantify leaf angle in 3D space regardless of leaf orientation relative to the camera, along with robustness to complex and varying outdoor conditions. By combining the PhenoBot platform with the AngleNet pipeline, the distribution of leaf angles across the canopy could be investigated nondestructively under natural conditions at multiple time points. Furthermore, this framework could easily be modified to measure the angles of other objects, such as sorghum plants and even trees in forestry studies. Beyond angle measurements, the concept of keypoint detection could be extended to length measurements, such as plant height and stem length.

Compared to traditional skeletonization methods, the major disadvantage of AngleNet is that it cannot deal with wavy-shaped leaves (Figure 15a). Since we focused on a small local area, the presence of a partially rolling leaf blade would result in a highly curved patch during the process of reprojecting a 2D line to a 3D point cloud, making it difficult and unreliable to fit the direction line in the resulting point cloud. This limitation could be overcome by performing keypoint detection on both left and right images and reconstructing the 3D line based on a pair of 2D line segments. Additionally, we observed that the 2D line was not exactly parallel to the direction of the midrib/stem (Figure 15b, left), which resulted in an inversible error for angle measurements in 3D space. Therefore, the keypoint locations and line directions should be refined before reprojecting to 3D coordinates. For example, locally straight contours (Lee et al., 2013) could be detected and used as a reference to adjust the line directions (Figure 15b, right).

5 | CONCLUSION

In this study, we employed an automated system to characterize leaf angle in agronomically grown maize plants in the field. A novel leaf angle detection and measurement pipeline, named AngleNet, was developed to obtain actual quantitative data for leaf angle throughout the entire height of the plant canopy. This pipeline utilizes an anchor-free CNN-based model to detect leaf angle and stereomatching algorithms to quantify leaf angle in the reconstructed 3D point cloud. AngleNet models a leaf collar as a center point and detects a leaf angle as a triplet of three keypoints. The proposed method with the novel representation of leaf angle bypasses the complex procedures of individual plant and leaf segmentation. Based on the detection and reconstruction results, the AngleNet-derived leaf angle and the associated node height were highly correlated with ground truth. In addition, the framework was successfully implemented to explore the variation of leaf angle in shoot architecture of two maize inbred lines, B73 and Mo17. The results of quantitative

analysis were consistent with the actual leaf angle distributions along plant height in these lines. Specifically, B73 has more erect architecture in the upper top canopy than Mo17. Stereo vision with the proper customization represents a practical tool to rapidly acquire high-quality RGB images and measure plant morphology under field conditions. The proposed system represents a feasible way to automatically quantify leaf angle in maize plants in a nondestructive manner. In addition, this system provides a new strategy for breeders to optimize plant architecture toward a smart canopy in cereal crops through large-scale field experiments. In future work, we will further improve the detection efficiency by performing stereo matching on keypoints and develop advanced deep learning algorithms to potentially achieve leaf angle estimation for partially occluded leaves.

ACKNOWLEDGMENTS

This project was funded by the US National Science Foundation Major Research Instrumentation Program (Award No: 1625364) and the Plant Sciences Institute at Iowa State University. This research is also a product of the Iowa Agriculture Experiment Station, Ames, Iowa, Project No. IOW03712, which is partially supported by Hatch Act and State of Iowa funds. We thank Taylor Tuel for his contributions to the design of PhenoBot and Gregory Schoenbaum for his assistance with field experiments. Open access funding provided by the Iowa State University Library.

DATA AVAILABILITY STATEMENT

The data that support the findings will be available upon reasonable request.

ORCID

Lie Tang http://orcid.org/0000-0002-8719-5378

REFERENCES

- Apelt, F., Breuer, D., Nikoloski, Z., Stitt, M. & Kragler, F. (2015) Phytotyping 4D: a light-field imaging system for non-invasive and accurate monitoring of spatio-temporal plant growth. *The Plant Journal*, 82, 693–706. https://doi.org/10.1111/tpj.12833
- Bao, Y., Tang, L., Breitzman, M.W., Salas Fernandez, M.G. & Schnable, P.S. (2019) Field-based robotic phenotyping of sorghum plant architecture using stereo vision. *Journal of Field Robotics*, 36(2), 397–415. Available from https://doi.org/10.1002/rob.21830
- Bao, Y., Tang, L., Srinivasan, S. & Schnable, P.S. (2019) Field-based architectural traits characterisation of maize plant using time-offlight 3D imaging. *Biosystems Engineering*, 178, 86–101. Available from https://doi.org/10.1016/j.biosystemseng.2018.11.005
- Cabrera-Bosquet, L., Fournier, C., Brichet, N., Welcker, C., Suard, B. & Tardieu, F. (2016) High-throughput estimation of incident light, light interception and radiation-use efficiency of thousands of plants in a phenotyping platform. *New Phytologist*, 212(1), 269–281. Available from https://doi.org/10.1111/nph.14027
- Chaivivatrakul, S., Tang, L., Dailey, M.N. & Nakarmi, A.D. (2014) Automatic morphological trait characterization for corn plants via 3D holographic reconstruction. *Computers and Electronics in Agriculture*, 109, 109–123. Available from https://doi.org/10.1016/J.COMPAG. 2014.09.005
- Che, Y., Wang, Q., Xie, Z., Zhou, L., Li, S., Hui, F. et al. (2020) Estimation of maize plant height and leaf area index dynamics using an unmanned

15564967, 0, Downloaded from https://onlinelibrary.wiley.com/doi/10.1002/rob.22166, Wiley Online Library on [01/07/2023]. See the Terms and Conditions (https://onlinelibrary.wiley.com/terms-and-conditions) on Wiley Online Library for rules of use; OA articles are governed by the applicable Cerative Commons License

- aerial vehicle with oblique and nadir photography. *Annals of Botany*, 126, 765–773. Available from https://doi.org/10.1093/aob/mcaa097
- Chen, M., Tang, Y., Zou, X., Huang, Z., Zhou, H. & Chen, S. (2021) 3D global mapping of large-scale unstructured orchard integrating eye-in-hand stereo vision and SLAM. Computers and Electronics in Agriculture, 187, 106237.
- Crick, C., Jay, G., Osentoski, S., Pitzer, B. & Jenkins, O.C. (2017) Rosbridge: ROS for non-ROS users. *Springer Tracts in Advanced Robotics*, 100, 493–504. Available from https://doi.org/10.1007/978-3-319-29363-9_28
- Das Choudhury, S., Bashyam, S., Qiu, Y., Samal, A. & Awada, T. (2018) Holistic and component plant phenotyping using temporal image sequence. *Plant methods*, 14(1), 35. Available from https://doi.org/ 10.1186/s13007-018-0303-x
- Duan, T., Chapman, S.C., Holland, E., Rebetzke, G.J., Guo, Y. & Zheng, B. (2016) Dynamic quantification of canopy structure to characterize early plant vigour in wheat genotypes. *Journal of Experimental Botany*, 67(15), 4523–4534. Available from https://doi.org/10. 1093/jxb/erw227
- Dzievit, M.J., Li, X. & Yu, J. (2019) Dissection of leaf angle variation in maize through genetic mapping and meta-analysis. *The Plant Genome*, 12, 180024. Available from https://doi.org/10.3835/plantgenome2018.05.0024
- Fischler, M.A. & Bolles, R.C. (1981) Random sample consensus: a paradigm for model fitting with applications to image analysis and automated cartography. *Communications of the ACM*, 24(6), 381–395. Available from https://doi.org/10.1145/358669.358692
- Ford, E.D., Cocke, A., Horton, L., Fellner, M. & Van Volkenburgh, E. (2008) Estimation, variation and importance of leaf curvature in *Zea mays* hybrids. *Agricultural and Forest Meteorology*, 148(10), 1598–1610. Available from https://doi.org/10.1016/j.agrformet.2008.05.015
- Furbank, R.T. & Tester, M. (2011) Phenomics-technologies to relieve the phenotyping bottleneck. *Trends in Plant Science*, 16(12), 635–644. Available from https://doi.org/10.1016/j.tplants.2011.09.005
- Gai, J. (2020). Navigation control of a robotic vehicle for field-based phenotyping (Doctoral dissertation, Iowa State University).
- Gai, J., Xiang, L. & Tang, L. (2021) Using a depth camera for crop row detection and mapping for under-canopy navigation of agricultural robotic vehicle. *Computers and Electronics in Agriculture*, 188, 106301. Available from https://doi.org/10.1016/j.compag.2021. 106301
- Gaillard, M., Miao, C., Schnable, J. & Benes, B. (2020) Sorghum segmentation by skeleton extraction. In *European Conference on Computer Vision*. Cham: Springer. pp. 296–311. https://doi.org/10. 1007/978-3-030-65414-6 21
- Gibbs, J.A., Pound, M., French, A.P., Wells, D.M., Murchie, E. & Pridmore, T. (2018) Plant phenotyping: an active vision cell for three-dimensional plant shoot reconstruction. *Plant Physiology*, 178(2), 524–534. Available from https://doi.org/10.1104/pp.18. 00664
- Hammer, G.L., Dong, Z., McLean, G., Doherty, A., Messina, C., Schussler, J. et al. (2009) Can changes in canopy and/or root system architecture explain historical maize yield trends in the U.S. corn belt? *Crop Science*, 49(1), 299–312. Available from https://doi.org/10.2135/cropsci2008.03.0152
- Hirschmuller, H. (2008) Stereo processing by semiglobal matching and mutual information. *IEEE Transactions on Pattern Analysis and Machine Intelligence*, 30(2), 328–341. Available from https://doi.org/10.1109/TPAMI.2007.1166
- Jiang, Y. & Li, C. (2020) Convolutional neural networks for image-based high-throughput plant phenotyping: a review. *Plant Phenomics*, 2020, 1–22. Available from https://doi.org/10.34133/2020/4152816
- Kenchanmane Raju, S.K., Adkins, M., Enersen, A., Santana de Carvalho, D., Studer, A.J., Ganapathysubramanian, B. et al. (2020) Leaf angle extractor: a high-throughput image processing framework for leaf

- angle measurements in maize and sorghum. *Applications in Plant Sciences*, 8(8), e11385. Available from https://doi.org/10.1002/aps3.11385
- Kingma, D.P. & Ba, J. (2014). Adam: a method for stochastic optimization. arXiv preprint arXiv:1412.6980. https://doi.org/10.48550/arXiv. 1412.6980
- Koirala, A., Walsh, K.B., Wang, Z. & McCarthy, C. (2019) Deep learning—method overview and review of use for fruit detection and yield estimation. Computers and Electronics in Agriculture, 162(April), 219–234. Available from https://doi.org/10.1016/j.compag.2019. 04.017
- Kong, T., Sun, F., Liu, H., Jiang, Y., Li, L. & Shi, J. (2020) Foveabox: beyond anchor-based object detection. *IEEE Transactions on Image Processing*, 29, 7389–7398. Available from https://doi.org/10. 1109/TIP.2020.3002345
- Law, H. & Deng, J. (2020) CornerNet: detecting objects as paired keypoints. *International Journal of Computer Vision*, 128(3), 642–656 http://arxiv.org/abs/1808.01244
- Lee, J.H., Zhang, G., Lim, J. & Suh, I.H. (2013). Place recognition using straight lines for vision-based SLAM. In: *Proceedings of IEEE International Conference on Robotics and Automation*, pp. 3799–3806. https://doi.org/10.1109/ICRA.2013.6631111
- Lewis, M.W., Bolduc, N., Hake, K., Htike, Y., Hay, A., Candela, H. et al. (2014) Gene regulatory interactions at lateral organ boundaries in maize. *Development*, 141(23), 4590–4597. Available from https://doi.org/10.1242/dev.111955
- Li, L., Yu, X., Zhang, S., Zhao, X. & Zhang, L. (2017) 3D cost aggregation with multiple minimum spanning trees for stereo matching. *Applied Optics*, 56(12), 3411. Available from https://doi.org/10.1364/ao.56. 003411
- Mansfield, B.D. & Mumm, R.H. (2014) Survey of plant density tolerance in U.S. maize germplasm. *Crop Science*, 54(1), 157–173. Available from https://doi.org/10.2135/cropsci2013.04.0252
- Mantilla-Perez, M.B., Bao, Y., Tang, L., Schnable, P.S. & Salas-Fernandez, M.G. (2020) Toward "smart canopy" sorghum: discovery of the genetic control of leaf angle across layers. *Plant Physiology*, 184, 1927–1940. Available from https://doi.org/10.1104/pp.20.00632
- Mccormick, R.F., Truong, S.K. & Mullet, J.E. (2016) 3D sorghum reconstructions from depth images identify QTL regulating shoot architecture. *Plant Physiology*, 172(October), 823–834. Available from https://doi.org/10.1104/pp.16.00948
- Mehltretter, M. & Heipke, C. (2021) Aleatoric uncertainty estimation for dense stereo matching via CNN-based cost volume analysisaleatoric uncertainty estimation for dense stereo matching via CNN-based cost volume analysis. ISPRS Journal of Photogrammetry and Remote Sensing, 171, 63-75. Available from https://doi.org/10.1016/j. isprsjprs.2020.11.003
- Newell, A., Yang, K. & Deng, J. (2016). Stacked hourglass networks for human pose estimation. In: European Conference on Computer Vision 9912 LNCS. pp. 483-499. https://doi.org/10.1007/978-3-319-46484-8 29
- Ort, D.R., Merchant, S.S., Alric, J., Barkan, A., Blankenship, R. E. & Zhu, X.G. (2015) Redesigning photosynthesis to sustainably meet global food and bioenergy demand. *Proceedings of the National Academy of Sciences of the United States of America*, 112(28), 8529–8536. https://doi.org/10.1073/pnas.1424031112
- Paszke, A., Gross, S., Chintala, S., Chanan, G., Yang, E., Facebook, Z.D. et al. (2017). Automatic differentiation in PyTorch.
- Pendleton, J.W., Smith, G.E., Winter, S.R. & Johnston, T.J. (1968) Field investigations of the relationships of leaf angle in corn (*Zea mays I.*) to grain yield and apparent photosynthesis 1. *Agronomy Journal*, 60(4), 422–424. Available from https://doi.org/10.2134/agronj 1968.00021962006000040027x
- Pérez-Borrero, I., Marín-santos, D., Gegúndez-arias, M.E. & Cortés-ancos, E. (2020) A fast and accurate deep learning method for strawberry

- instance segmentation. *Computers and Electronics in Agriculture*, 178(August), 105736. Available from https://doi.org/10.1016/j.compag.2020.105736
- Poggi, M., Tosi, F., Batsos, K., Mordohai, P. & Mattoccia, S. (2021). On the Synergies Between Machine Learning and Binocular Stereo for Depth Estimation From Images: A Survey. *IEEE Transactions on Pattern Analysis and Machine Intelligence*, 44(9), 5314–5334. https://doi.org/10.1109/TPAMI.2021.3070917
- Redmon, J. & Farhadi, A. (2018). YOLOv3: an incremental improvement.

 ArXiv preprint arXiv:1804.02767. https://doi.org/10.48550/arXiv.
 1804.02767
- Ren, S., He, K., Girshick, R. & Sun, J. (2017) Faster R-CNN: towards real-time object detection with region proposal networks. *IEEE Transactions on Pattern Analysis and Machine Intelligence*, 39(6), 1137–1149. Available from https://doi.org/10.1109/TPAMI.2016. 2577031
- Russell, W.A. (1972) Registration of B70 and B73 parental lines of maize 1 (Reg. Nos. PL16 and PL17). *Crop Science*, 12(5), 721. Available from https://doi.org/10.2135/cropsci1972.0011183x001200050085x
- Santos, T.T., de Souza, L.L., dos Santos, A.A. & Avila, S. (2020) Grape detection, segmentation, and tracking using deep neural networks and three-dimensional association. *Computers and Electronics in Agriculture*, 170(February), 105247. Available from https://doi.org/ 10.1016/j.compag.2020.105247
- Souza, A. & Yang, Y. (2021) High-Throughput corn image segmentation and trait extraction using chlorophyll fluorescence images. *Plant Phenomics*, 2021. Available from https://doi.org/10.34133/2021/ 9792582
- Stanford Artificial Intelligence Laboratory (2018) *Robotic operating system*. Available from https://www.ros.org/
- Sun, S., Li, C., Chee, P.W., Paterson, A.H., Jiang, Y., Xu, R. et al. (2020) Three-dimensional photogrammetric mapping of cotton bolls in situ based on point cloud segmentation and clustering. ISPRS Journal of Photogrammetry and Remote Sensing, 160, 195–207. Available from https://doi.org/10.1016/j.isprsjprs.2019.12.011
- Tang, D., Chen, Z., Ni, J., Jiang, Q., Li, P., Wang, L. et al. (2018). Identification of QTL for leaf angle at canopy-wide levels in maize. In bioRxiv (p. 499665). bioRxiv. https://doi.org/10.1101/499665
- Tang, Y., Chen, M., Wang, C., Luo, L., Li, J., Lian, G. et al. (2020) Recognition and localization methods for vision-based fruit picking robots: a review. Frontiers in Plant Science, 11, 510.
- Thapa, S., Zhu, F., Walia, H., Yu, H. & Ge, Y. (2018). A novel LiDAR-based instrument for high-throughput, 3D measurement of morphological traits in maize and sorghum. https://doi.org/10.3390/s18041187
- Toris, R., Kammerl, J., Lu, D.V., Lee, J., Jenkins, O.C., Osentoski, S. et al. (2015). Robot Web Tools: efficient messaging for cloud robotics. In: *IEEE International Conference on Intelligent Robots and Systems* 2015-December. pp. 4530-4537. https://doi.org/10.1109/IROS. 2015.7354021
- Truong, S.K., Mccormick, R.F., Rooney, W.L. & Mullet, J.E. (2015) Harnessing genetic variation in leaf angle to increase productivity of sorghum bicolor. *Genetics*, 201(3), 1229–1238. https://doi.org/10.1534/genetics.115.178608
- Tuel, T.L. (2019). A robotic proximal sensing platform for in-field highthroughput crop phenotyping (Master's thesis, Iowa State University).
- Vit, A., Shani, G. & Bar-hillel, A. (2020) Length phenotyping with interest point detection. Computers and Electronics in Agriculture, 176(July), 105629. Available from https://doi.org/10.1016/j.compag.2020. 105629
- Wang, N., Cao, D., Gong, F., Ku, L., Chen, Y. & Wang, W. (2015) Differences in properties and proteomes of the midribs contribute to the size of the leaf angle in two near-isogenic maize lines. *Journal of Proteomics*, 128, 113–122. Available from https://doi.org/10.1016/j.jprot.2015.07.027

- Wang, Y., Wen, W., Wu, S., Wang, C., Yu, Z., & Guo, X. et al. (2019) Maize plant phenotyping: comparing 3D laser scanning, multi-view stereo reconstruction, and 3D digitizing estimates. *Remote Sensing*, 11(1), 63. Available from https://doi.org/10.3390/rs11010063
- Wei, H., Zhang, Y., Chang, Z., Li, H., Wang, H. & Sun, X. (2020) Oriented objects as pairs of middle lines. ISPRS Journal of Photogrammetry and Remote Sensing, 169(July), 268–279. Available from https://doi.org/ 10.1016/j.isprsjprs.2020.09.022
- Wu, S., Wen, W., Wang, Y., Fan, J., Wang, C., Gou, W. et al. (2020) MVS-Pheno: a portable and low-cost phenotyping platform for maize shoots using multiview stereo 3D reconstruction. *Plant Phenomics*, 2020, 1–17. Available from https://doi.org/10.34133/2020/1848437
- Wu, S., Wen, W., Xiao, B., Guo, X., Du, J., Wang, C. et al. (2019) An accurate skeleton extraction approach from 3D point clouds of maize plants. Frontiers in Plant Science, 10, 248. Available from https://doi.org/10.3389/fpls.2019.00248
- Xiang, L., Bao, Y., Tang, L., Ortiz, D. & Salas-Fernandez, M.G. (2019) Automated morphological traits extraction for sorghum plants via 3D point cloud data analysis. *Computers and Electronics in Agriculture*, 162, 951–961. Available from https://doi.org/10.1016/j.compag. 2019.05.043
- Xiang, L., Tang, L., Gai, J. & Wang, L. (2020). PhenoStereo: a high-throughput stereo vision system for field-based plant phenotyping With an application in sorghum stem diameter estimation. In: ASABE 2020 Annual International Meeting. https://doi.org/10.13031/aim. 202001190
- Yu, F., Wang, D., Shelhamer, E. & Darrell, T. (2017). Deep layer aggregation. In: Proceedings of the IEEE Computer Society Conference on Computer Vision and Pattern Recognition. pp. 2403–2412. http:// arxiv.org/abs/1707.06484
- Zbontar, J. & Lecun, Y. (2016) Stereo matching by training a convolutional neural network to compare image patches. *Journal of Machine Learning Research*, 17(65), 1–32. Available from https://jmlr.org/papers/v17/15-535.html
- Zermas, D., Morellas, V., Mulla, D. & Papanikolopoulos, N. (2020) 3D model processing for high throughput phenotype extraction—the case of corn. Computers and Electronics in Agriculture, 172, 105047. Available from https://doi.org/10.1016/j.compag.2019.105047
- Zhang, X., Huang, C., Wu, D., Qiao, F., Li, W., Duan, L. et al. (2017) High-throughput phenotyping and QTL mapping reveals the genetic architecture of maize plant growth. *Plant Physiology*, 173(3), 1554–1564. Available from https://doi.org/10.1104/pp.16.01516
- Zhang, Y., Sun, H., Zuo, J., Wang, H., Xu, G. & Sun, X. (2018) Aircraft type recognition in remote sensing images based on feature learning with conditional generative adversarial networks. *Remote Sensing*, 10(7), 1123. Available from https://doi.org/10.3390/ rs10071123
- Zhao, X., Fang, P., Zhang, J. & Peng, Y. (2018). QTL mapping for six ear leaf architecture traits under water-stressed and well-watered conditions in maize (*Zea mays L.*). *Plant Breeding*, 137(1), 60–72. Available from https://doi.org/10.1111/pbr.12559
- Zhou, X., Wang, D. & Krähenbühl, P. (2019). Objects as points. ArXiv preprint arXiv:1904.07850. http://arxiv.org/abs/1904.07850
- Zhu, C., Miao, T., Xu, T., Yang, T. & Li, N. (2020). Stem-leaf segmentation and phenotypic trait extraction of maize shoots from three-dimensional point cloud. *ArXiv preprint arXiv*:2009.03108. https://arxiv.org/abs/2009.03108
- Zhu, X.-G., Long, S.P. & Ort, D.R. (2010) Improving photosynthetic efficiency for greater yield. Annual Review of Plant Biology, 61(1), 235–261. Available from https://doi.org/10.1146/annurev-arplant-042809-112206
- Zou, H., Lu, H., Li, Y., Liu, L. & Cao, Z. (2020) Maize tassels detection: A benchmark of the state of the art. *Plant Methods*, 16(1), 108. Available from https://doi.org/10.1186/s13007-020-00651-z

Zuber, M.S. (1973) Registration of 20 maize parental Lines1(Reg. Numbers PL 18 to 37). *Crop Science*, 13(6), 779–780. Available from https://doi.org/10.2135/cropsci1973.0011183x001300060085x

SUPPORTING INFORMATION

Additional supporting information can be found online in the Supporting Information section at the end of this article.

How to cite this article: Xiang, L., Gai, J., Bao, Y., Yu, J., Schnable, P. S. & Tang, L. (2023) Field-based robotic leaf angle detection and characterization of maize plants using stereo vision and deep convolutional neural networks. *Journal of Field Robotics*, 1–20. https://doi.org/10.1002/rob.22166